$$F_1^2(\theta) = \tfrac{3}{2}[S_{Mn}(S_{Mn}+1)S_{Rad}(S_{Rad}+1)]^{1/2}\sin^2\theta\cos^2\theta\,(\omega_d^2V^2)$$

$$F_2^2(\theta) = \tfrac{3}{4}[S_{Mn}(S_{Mn}+1)S_{Rad}(S_{Rad}+1)]^{1/2}\sin^4\theta\,(\omega_d^2V^2)$$

$$\omega_d = \frac{\hbar\gamma_e^2}{C^3} \qquad V = \sum_{ij}\left|\frac{C}{r_{ij}}\right|^3$$

C is the distance between manganese(II) and radical spins in the hypothesis of point dipole (C = 2.82 Å), and V has been calculated for simplicity in the case of a perfectly straight chain.

(10) shows that ω_c is angular dependent; therefore, close insight of the cutoff mechanism would be obtained from the oriented spin-lattice relaxation rates in the low-frequency range. Unfortunately, the small size of the crystals and the reduced NMR spectrometer sensitivity at low frequencies prevented us from exploring the low-frequency range for the oriented crystals. Nevertheless, also from the powders we can get useful information calculating the cutoff frequency assuming that it is dominated by the crystallites with $\theta = 90°$. In this way, we calculate $\nu_c = \omega_c/2\pi \cong 19$ MHz by using the theoretical $D = 1.16\omega_{ex}$ value, while we calculate $\nu_c \cong 15$ MHz by using the D value obtained from the fitting of the single-crystal data, in good agreement with the experimental values ($\nu_c \cong 17$ MHz for ^{1}H and 22 MHz for ^{19}F). The decrease of T_1^{-1} at low frequency is the consequence of the fact that ω_c is frequency dependent with a $\omega^{-1/2}$ law, and of the large contribution of the $A^2j(\omega_n)$ term to the relaxation rate.

The calculations indicate that the cutoff effects can be satisfactorily justified by the dipolar interactions between spins of the same chain. This result is very important because it puts an upper limit on the value of the interchain exchange interaction to $J' \cong 6 \times 10^{-4}$ cm^{-1}. The J'/J ratio is so much smaller than 2×10^{-6}, which confirms the exceptionally good one-dimensional nature of Mn(hfac)$_2$(NITiPr).

Conclusions

In this paper, we have shown how NMR is a powerful tool for the analysis of the magnetic properties of one-dimensional magnetic materials. Theory had already been tested on ferromagnets and antiferromagnets,[24-28] but this is the first example of the successful analysis of a one-dimensional ferrimagnet. In particular, we have confirmed that in Mn(hfac)$_2$(NITiPr) the interchain exchange interactions are exceedingly small, therefore supporting our analysis of the mechanism of transition to three-dimensional order driven by dipolar interactions. The NMR data confirm that at high temperature Mn(hfac)$_2$(NITiPr) is a textbook example of a one-dimensional ferrimagnet as was already suggested on the basis of the EPR spectra.

The numerous one-dimensional magnetic materials that have been recently synthesized by using a molecular approach may be usefully tested with NMR experiments in order to better understand their magnetic properties. Further these materials with many chemically not equivalent protons might also provide the opportunity to observe more than one signal per nucleus, thus providing more refined testing grounds for the theories of spin dynamics in one-dimensional materials. Finally the experiments may be performed also in the vicinity of the transition temperature to three-dimensional magnetic order to obtain insight into the critical fluctuations and the field dependence of the critical temperatures. We are currently working along these lines.

Acknowledgment. Thanks are due to Professor A. Rigamonti, University of Pavia, for constant help in the interpretation of the magnetic data. Stimulating discussions with Professors I. Bertini, University of Florence, and C. Luchinat, University of Bologna, are gratefully acknowledged. The financial support of MURST and of the "Progetto Finalizzato Materiali Speciali per Tecnologie Avanzate" is gratefully acknowledged.

Artificial Manipulation of Apparent Bond Lengths As Determined by Single-Crystal X-ray Diffraction

Keum Yoon and Gerard Parkin*

Contribution from the Department of Chemistry, Columbia University, New York, New York 10027. *Received April 17, 1991*

Abstract: Single crystals composed of solid solutions of pairs of the complexes {η^3-HB(3-Bu^{t}pz)$_3$}ZnCl, {η^3-HB(3-Bu^{t}pz)$_3$}ZnI, and {η^3-HB(3-Bu^{t}pz)$_3$}ZnCH$_3$ [3-Bu^{t}pz = 3-$C_3N_2H_2Bu^t$], over a range of compositions, have been examined by X-ray diffraction. In each case the presence of the impurity is manifested by the observation of an apparent Zn-X bond length that is intermediate between the two possible extremes for the pair of complexes involved. As expected the relationship between the apparent bond length and composition is not linear but is weighted by the relative scattering powers of the disordered groups.

Single-crystal X-ray diffraction is the most widely used technique for the determination of both (i) molecular structures and (ii) accurate bond lengths of complexes in the solid state. However, the occurrence of crystallographic disorder derived from packing identical molecules in different, though structurally similar, orientations may result in the incorrect determination of not only bond lengths but also molecular structures. For example, the molecular structure of the ethylidyne complex W(PMe$_3$)$_4$(CH$_3$)(CCH$_3$) was originally incorrectly assigned as the *dimethyl* derivative W(PMe$_3$)$_4$(CH$_3$)$_2$, as a result of disorder between the ethylidyne and methyl ligands.[1] Disorder of groups that have similar steric requirements (e.g., pairs of atoms) is more common, as illustrated by the example of {η^3-HB(pz)$_3$}Mo(O)Cl$_2$, which shows three different Mo-X bond lengths that are intermediate between Mo=O and Mo-Cl, with none representing either a pure Mo=O or Mo-Cl bond length.[2] A second type of disorder occurs when a *nonidentical*, but structurally related, molecule occupies sites in the crystal lattice. However, even though cocrystallization of isostructural molecules is well-established,[3] the extent of this phenomenon does not appear to be widely appreciated, in part

(1) (a) Jones, R. A.; Wilkinson, G.; Galas, A. M. R.; Hursthouse, M. B. *J. Chem. Soc., Chem. Commun.* **1979**, 926-927. (b) Chiu, K. W.; Jones, R. A.; Wilkinson, G.; Galas, A. M. R.; Hursthouse, M. B.; Malik, K. M. A. *J. Chem. Soc., Dalton Trans.* **1981**, 1204-1211.

(2) Lincoln, S.; Koch, S. A. *Inorg. Chem.* **1986**, *25*, 1594-1602.

(3) For example, doping of paramagnetic materials into crystals of isostructural diamagentic complexes is used exclusively in single-crystal EPR strudies. See, for example: (a) Peterson, J. L.; Dahl, L. F. *J. Am. Chem. Soc.* **1975**, *97*, 6416-6422. (b) Petersen, J. L.; Dahl, L. F. *J. Am. Chem. Soc.* **1975**, *97*, 6422-6433.

0002-7863/91/1513-8414$02.50/0

Table I. Selected Bond Lengths (Å) and Angles (deg) for $\{\eta^3\text{-HB(3-Bu}^t\text{pz)}_3\}$ZnX (X = Cl, Br, I, CH_3)

	$\{\eta^3\text{-HB(3-Bu}^t\text{pz)}_3\}$ZnCl	$\{\eta^3\text{-HB(3-Bu}^t\text{pz)}_3\}$ZnBr	$\{\eta^3\text{-HB(3-Bu}^t\text{pz)}_3\}$ZnI	$\{\eta^3\text{-HB(3-Bu}^t\text{pz)}_3\}$ZnCH$_3$
Zn–X	2.183 (2)	2.325 (1)	2.518 (1)	1.971 (4)
Zn–N(12)	2.045 (4)	2.057 (5)	2.073 (5)	2.109 (4)
Zn–N(22)	2.054 (3)	2.060 (4)	2.068 (3)	2.109 (2)
X–Zn–N(12)	121.3 (1)	121.0 (2)	120.3 (1)	123.1 (2)
X–Zn–N(22)	122.5 (1)	122.7 (1)	123.1 (1)	125.3 (1)
N(12)–Zn–N(22)	94.6 (1)	94.7 (1)	95.2 (1)	91.4 (1)
N(22)–Zn–N(22′)	94.1 (2)	93.8 (2)	92.6 (2)	90.1 (1)

Table II. Apparent Bond Lengths as a Function of Composition

composition[a]	d(Zn–L),[b] Å	composition[a]	d(Zn–L),[b] Å	composition[a]	d(Zn–L),[b] Å
[Zn]Cl	2.183 (2)	[Zn]CH$_3$	1.971 (4)	[Zn]CH$_3$	1.971 (4)
[Zn]Cl$_{0.98}$I$_{0.02}$	2.198 (1)	[Zn](CH$_3$)$_{0.88}$Cl$_{0.12}$	2.049 (4)	[Zn](CH$_3$)$_{0.93}$I$_{0.07}$	2.209 (3)
[Zn]Cl$_{0.89}$I$_{0.11}$	2.261 (1)	[Zn](CH$_3$)$_{0.64}$Cl$_{0.36}$	2.105 (2)	[Zn](CH$_3$)$_{0.93}$I$_{0.07}$	2.216 (3)
[Zn]Cl$_{0.71}$I$_{0.29}$	2.358 (1)	[Zn](CH$_3$)$_{0.56}$Cl$_{0.44}$	2.118 (3)	[Zn](CH$_3$)$_{0.92}$I$_{0.08}$	2.203 (3)
[Zn]Cl$_{0.50}$I$_{0.50}$	2.421 (1)	[Zn](CH$_3$)$_{0.54}$Cl$_{0.46}$	2.123 (2)	[Zn](CH$_3$)$_{0.31}$I$_{0.69}$	2.467 (1)
[Zn]Cl$_{0.38}$I$_{0.62}$	2.446 (1)	[Zn](CH$_3$)$_{0.46}$Cl$_{0.54}$	2.136 (3)	[Zn](CH$_3$)$_{0.09}$I$_{0.91}$	2.508 (1)
[Zn]Cl$_{0.18}$I$_{0.82}$	2.494 (1)	[Zn]Cl	2.183 (2)	[Zn]I	2.518 (1)
[Zn]I	2.518 (1)				

[a] [Zn] = $\{\eta^3\text{-HB(3-Bu}^t\text{pz)}_3\}$Zn. Compositions were determined by ^{1}H NMR analysis of the crystal. In most cases similar compositions were also measured for the bulk sample. [b] The Zn–L (L = $X_{(1-n)}Y_n$) bond lengths listed are those for a model in which the coordinates of a single composite atom (L) are refined at the disordered site.

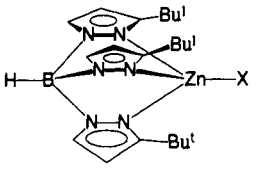

Figure 1. Molecular structure of $\{\eta^3\text{-HB(3-Bu}^t\text{pz)}_3\}$ZnX.

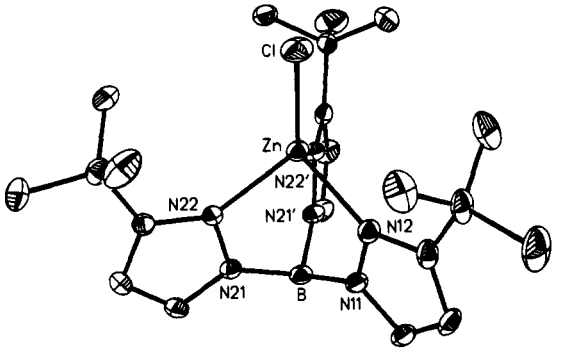

Figure 2. ORTEP drawing of $\{\eta^3\text{-HB(3-Bu}^t\text{pz)}_3\}$ZnCl.

due to the common belief that single crystals are invariably pure compounds. In this regard, we have recently demonstrated that the original report of "distortional"[4] or "bond-stretch"[5] isomers, molecules that differ only by the length of one or more bonds, is one such example of crystallographic disorder with nonidentical molecules. Thus, the observation of blue and green "isomers" of *cis-mer*-$MoOCl_2(PMe_2Ph)_3$, whose significant difference lies only in the length of the Mo=O bonds,[4] is in fact a result of co-crystallization of the blue oxo complex with small quantities of the isostructural yellow trichloride complex *mer*-$MoCl_3(PMe_2Ph)_3$.[6] Furthermore, the surprising observation of two significantly distinct Hf–CH_3 bond lengths [2.381 (8) and 2.382 (7) Å][7] in the otherwise symmetric molecule $(\eta^5\text{-}C_5H_5)_2Hf(CH_3)_2$ has been reinterpreted as arising from cocrystallization with the chloride derivative $(\eta^5\text{-}C_5H_5)_2Hf(CH_3)Cl$.[8] Here we report our investigations on the artificial manipulation of apparent bond lengths by doping with impurities, in order to further demonstrate the generality of this phenomenon and also to quantify the effect.

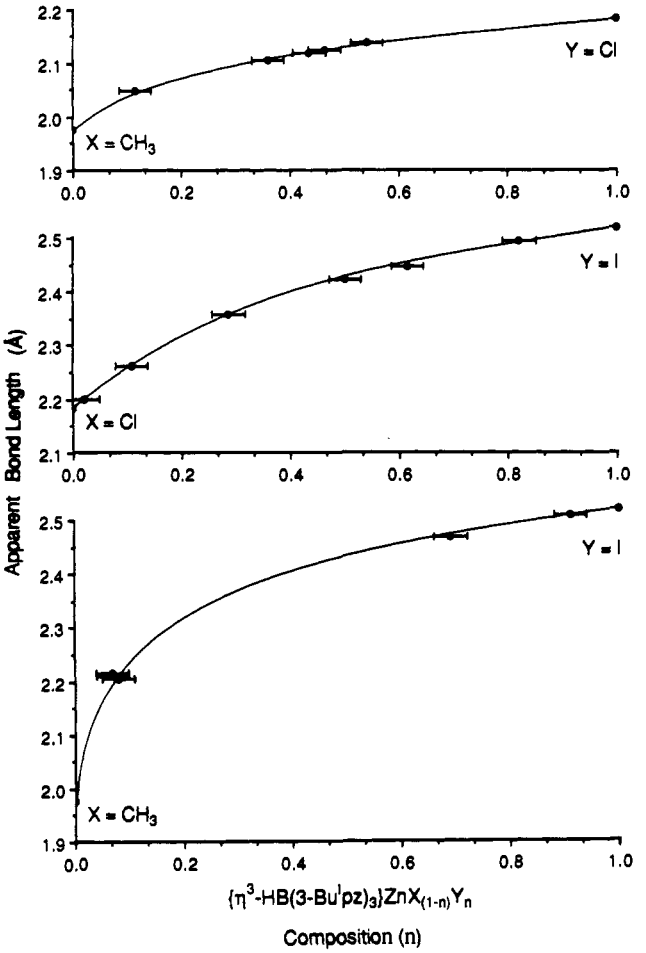

Figure 3. Variation in apparent bond length as a function of composition.

(4) (a) Chatt, J.; Manojlovic-Muir, L.; Muir, K. W. *Chem. Commun.* **1971**, 655–656. (b) Manojlovic-Muir, L. *J. Chem. Soc. (A)* **1971**, 2796–2800. (c) Manojlovic-Muir, L.; Muir, K. W. *J. Chem. Soc., Dalton Trans.* **1972**, 686–690. (d) Haymore, B. L.; Goddard, W. A., III; Allison, J. N. *Proc. Int. Conf. Coord. Chem., 23rd* **1984**, 535.

(5) (a) Jean, Y.; Lledos, A.; Burdett, J. K.; Hoffmann, R. *J. Am. Chem. Soc.* **1988**, *110*, 4506–4516. (b) Jean, Y.; Lledos, A.; Burdett, J. K.; Hoffmann, R. *J. Chem. Soc., Chem. Commun.* **1988**, 140–142.

(6) Yoon, K.; Parkin, G.; Rheingold, A. L. *J. Am. Chem. Soc.* **1991**, *113*, 1437–1438.

(7) Fronczek, F. R.; Baker, E. C.; Sharp, P. R.; Raymond, K. N.; Alt, H. G.; Rausch, M. D. *Inorg. Chem.* **1976**, *15*, 2284–2289.

(8) Hunter, W. E.; Hrncir, D. C.; Bynum, R. V.; Penttila, R. A.; Atwood, J. L. *Organometallics* **1983**, *2*, 750–755.

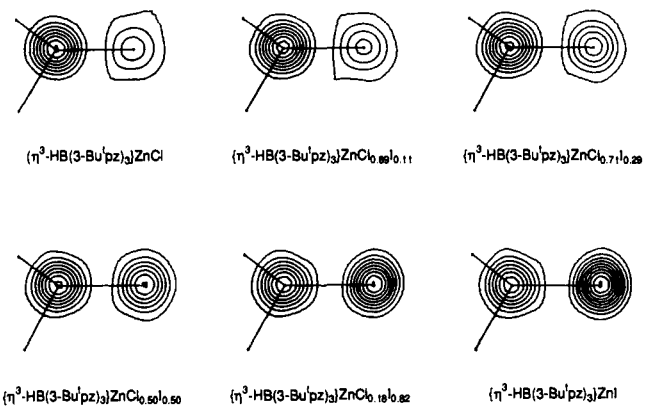

Figure 4. Electron density contours in the plane N(12)–Zn–$Cl_{1-n}I_n$ illustrating the change in electron density at the disordered site for a selection of the series $\{\eta^3$-HB(3-Bu'pz)$_3\}$ZnCl$_{1-n}$I$_n$. The solid lines indicate bonds to zinc.

Results and Discussion

We have recently reported a series of tris(3-*tert*-butylpyrazolyl)hydroboratozinc complexes, $\{\eta^3$-HB(3-Bu'pz)$_3\}$ZnX (3-Bu'pz = 3-$C_3N_2H_2$Bu'; X = H, R, Cl, I, SH, O_2CH, O_2CR),[9] in which the tripod ligand confers considerable stability and crystallinity to the complexes (Figure 1). The molecular structures of the complexes $\{\eta^3$-HB(3-Bu'pz)$_3\}$ZnX (X = Cl, Br, I, CH_3) have been determined by single-crystal X-ray diffraction, as illustrated by the representative example $\{\eta^3$-HB(3-Bu'pz)$_3\}$ZnCl as shown in Figure 2. Selected bond lengths and angles for all the complexes are given in Table I. Such as series of structurally related complexes provides a well-defined system that would allow us to quantify the effect of impurities upon observed apparent bond lengths. Specifically, we have examined single crystals composed of pairs of the complexes $\{\eta^3$-HB(3-Bu'pz)$_3\}$ZnCl, $\{\eta^3$-HB(3-Bu'pz)$_3\}$ZnI, and $\{\eta^3$-HB(3-Bu'pz)$_3\}$ZnCH$_3$, over a range of compositions. In each case, only a single "atom" is observed at the disordered site, corresponding to an *apparent* Zn–X bond length that is a composite for the pair of complexes concerned. The results of these studies are illustrated in Table II and Figure 3 which quantify the relationship between the observed apparent bond length and composition. Furthermore, the electron density maps for the series of complexes $\{\eta^3$-HB(3-Bu'pz)$_3\}$ZnCl$_{1-n}$I$_n$, shown in Figure 4, indicate how only a single maximum in electron density is observed at the disordered site. The above results show that, as expected, the relationship between the apparent bond length and composition is not linear but is weighted by the relative scattering powers of the disordered groups. The most significant deviation from linearity occurs when there is considerable disparity between the scattering powers of the disordered groups, with the group of the higher scattering power contributing most to the apparent bond length. Thus, small quantities of iodide impurities have a pronounced effect on observed apparent bond lengths.

The presence of impurities in a single crystal is often signalled by the observation of abnormal temperature factors for the atoms concerned. However, we have observed that reasonable thermal parameters can be observed at impurity levels that are sufficient to result in a significant apparent change in the true bond length. Thus, Figure 5 illustrates how the thermal parameters for the series of complexes $\{\eta^3$-HB(3-Bu'pz)$_3\}$ZnCl$_{1-n}$I$_n$ vary when refined as (i) Cl only, (ii) I only, and (iii) a composite atom (L = $Cl_{1-n}I_n$) in which the site occupancies have been allowed to refine. For reference, the ORTEP diagrams of the pure $\{\eta^3$-HB(3-Bu'pz)$_3\}$ZnCl and $\{\eta^3$-HB(3-Bu'pz)$_3\}$ZnI complexes are also included in Figure 5. Refining the disordered site as Cl results in the expected pronounced shrinking of the thermal ellipsoid as the iodide content (and hence increased electron density) at the disordered site increases. Similarly, refining the disordered site as I results in the expected expansion of the thermal ellipsoid as the iodide content decreases. Unacceptable thermal parameters are clearly obtained when either (i) the composition is iodide-rich and the site is refined as Cl or (ii) the composition is chloride-rich and the site is refined as I. However, it can be seen that reasonable thermal parameters can be observed at impurity levels that are low but which are significant enough to result in a change in apparent bond length. Thus, the observation of "normal" thermal parameters is not necessarily a good indicator that the crystal is pure, and consequently that the observed bond length is correct, even though it may be determined with high precision and apparent accuracy.

The result of refining the disordered site as a composite atom (L = $C_{1-n}I_n$), also shown in Figure 5, demonstrates that expansion of the thermal ellipsoid along the bond vector, which may have been expected because the disordered atoms are located at different positions along this vector, is *not* observed for the $\{\eta^3$-HB(3-Bu'pz)$_3\}$ZnCl$_{1-n}$I$_n$ system. This observation reiterates the suggestion that the observation of "normal" thermal parameters is not necessarily a good indicator that an observed bond length is correct. Testament to this suggestion is provided by the result of refining the disordered site of the crystal of composition $\{\eta^3$-HB(3-Bu'pz)$_3\}$ZnCl$_{0.5}$I$_{0.5}$ as *bromine*, as shown in Figure 6. Clearly, a perfectly acceptable ORTEP drawing can be produced for the complex $\{\eta^3$-HB(3-Bu'pz)$_3\}$ZnBr, even though the crystal studied contained *no bromine*. For comparison, Figure 6 also shows the ORTEP drawing for authentic $\{\eta^3$-HB(3-Bu'pz)$_3\}$ZnBr, which indicates the extremely close similarity with the "artificial" bromide $\{\eta^3$-HB(3-Bu'pz)$_3\}$ZnCl$_{0.5}$I$_{0.5}$. Indeed, without prior knowledge, it would be difficult to distinguish which one of the pair of ORTEP drawings shown in Figure 6 corresponds to the authentic compound $\{\eta^3$-HB(3-Bu'pz)$_3\}$ZnBr.

A consideration of resolution is central to the problems arising from disordered structures. Stenkamp and Jensen have suggested that the limit of resolution for point atoms in three-dimensional electron density maps is 0.917 d_{min} (where $d_{min} = \lambda/2\sin\theta$). In view of thermal motion, the limit of resolution would be expected to be somewhat greater than that expressed by 0.917d_{min}. The resolution is calculated to be 0.71 Å for data collected out to $2\theta_{max}$ = 55° with Mo radiation (λ = 0.71073 Å), a typical value for our experiments. The distance between the disordered atoms in the system that we have studied ranges from 0.20 Å for $\{\eta^3$-HB(3-Bu'pz)$_3\}$ZnCH$_3$ and $\{\eta^3$-HB(3-Bu'pz)$_3\}$ZnCl to 0.54 Å for $\{\eta^3$-HB(3-Bu'pz)$_3\}$ZnCH$_3$ and $\{\eta^3$-HB(3-Bu'pz)$_3\}$ZnI. Thus, it is not surprising that the disorder could not be resolved for our system, even for the case of a 50:50 mixture, $\{\eta^3$-HB(3-Bu'pz)$_3\}$ZnCl$_{0.5}$I$_{0.5}$.[11] However, we do note that previous work has shown that disordered groups such as chloride and iodide may be refined under favorable circumstances.[12,13]

Conclusion

In conclusion, the results of this study clearly underscore the importance of crystal purity in the determination of correct bond lengths. Thus, cocrystallization may result in the observation of incorrect bond lengths, even though they may be determined both with high precision and apparent accuracy. We have provided further examples that indicate the generality in which cocrystallization with small amounts of impurities results in significant changes in apparent bond lengths and have also quantified this effect. While cocrystallization is likely to be most common when

(9) (a) Gorrell, I. B.; Looney, A.; Parkin, G. *J. Chem. Soc., Chem. Commun.* **1990**, 220–222. (b) Han, R.; Gorrell, I. B.; Looney, A. G.; Parkin, G. *J. Chem. Soc., Chem. Commun.* **1991**, 717–719.

(10) Stenkamp, R. E.; Jensen, L. H. *Acta Crystallogr.* **1984**, *A40*, 251–254.

(11) Although our data could not resolve the disorder, a better crystallographic model for our system would be to place and refine two partial-occupancy atoms located at different positions along the bond vector. However, this method is often unsuccessful since the partial atoms tend to converge to the same position (for example, see ref 2).

(12) (a) Bianconi, P. A.; Vrtis, R. N.; Rao, C. P.; Williams, I. D.; Engeler, M. P.; Lippard, S. J. *Organometallics* **1987**, *6*, 1968–1977. (b) Lam, C. T.; Lewis, D. L.; Lippard, S. J. *Inorg. Chem.* **1976**, *15*, 989–991.

(13) (a) Davis, B. R.; Ibers, J. A. *Inorg. Chem.* **1971**, *10*, 578–585. (b) Carmona, E.; Marin, J. M.; Poveda, M. L.; Atwood, J. L.; Rogers, R. D. *Polyhedron* **1983**, *2*, 185–193.

Table III. Summary of Crystal and Intensity Collection Data

	$\{\eta^3$-HB(3-Bu^{t}pz)$_3\}$ZnCl	$\{\eta^3$-HB(3-Bu^{t}pz)$_3\}$ZnBr	$\{\eta^3$-HB(3-Bu^{t}pz)$_3\}$ZnI	$\{\eta^3$-HB(3-Bu^{t}pz)$_3\}$ZnCH$_3$
formula	$C_{21}H_{34}N_6BZnCl$	$C_{21}H_{34}N_6BZnBr$	$C_{21}H_{34}N_6BZnI$	$C_{22}H_{37}N_6BZn$
formula wt	482.2	526.6	573.6	461.8
lattice	orthorhombic	orthorhombic	orthorhombic	orthorhombic
cell constants				
a (Å)	16.029 (5)	16.130 (6)	16.443 (3)	16.297 (4)
b (Å)	15.975 (5)	15.921 (8)	15.848 (5)	15.882 (4)
c (Å)	9.786 (2)	9.822 (3)	9.927 (2)	9.757 (2)
V (Å^3)	2506 (1)	2522 (2)	2587 (1)	2525 (1)
Z	4	4	4	4
space group	*Pnma* (no. 62)	*Pnma* (no. 62)	*Pnma* (no. 62)	*Pnma* (no. 62)
radiation (λ, Å)	Mo Kα (0.71073)	Mo Kα (0.71073)	Mo Kα (0.71073)	Mo Kα (0.71073)
ρ (calcd) (g cm^{-3})	1.28	1.39	1.47	1.21
goodness of fit	1.540	1.123	1.171	1.309
R	0.0443	0.0408	0.0392	0.0413
R_w	0.0375	0.0490	0.0501	0.0454

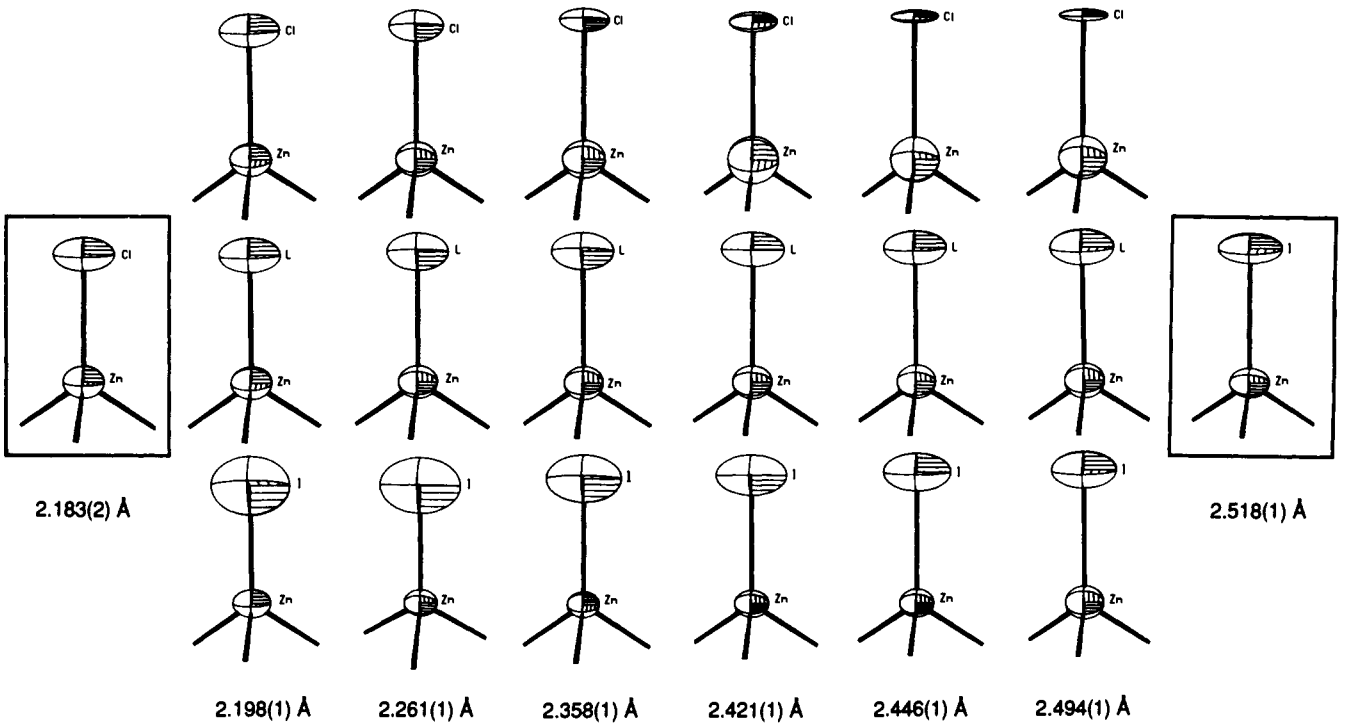

Figure 5. Thermal ellipsoids for the series $\{\eta^3$-HB(3-Bu^{t}pz)$_3\}$ZnCl$_{1-n}$I$_n$ as the result of refining as (i) Cl (upper row), (ii) I (lower row), and (iii) a composite atom (middle row).

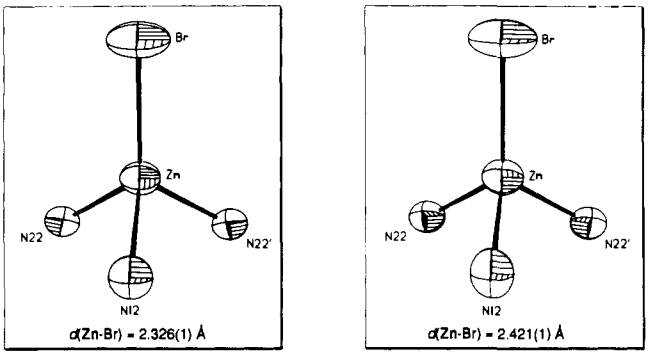

Figure 6. Comparison of thermal parameters of the disordered structure $\{\eta^3$-HB(3-Bu^{t}pz)$_3\}$ZnCl$_{0.5}$I$_{0.5}$ when refined as $\{\eta^3$-HB(3-Bu^{t}pz)$_3\}$ZnBr, with that of authentic $\{\eta^3$-HB(3-Bu^{t}pz)$_3\}$ZnBr.

the molecules are structurally similar, e.g., chloride and iodide derivatives, cocrystallization between methyl and halide ligands also occurs readily. The relevance of this latter example can be seen upon consideration of the fact that methyl derivatives are generally prepared by alkylation of a metal–*halide* complex.[14] Disorder between structurally unrelated groups is also possible (for example CH_3 and CCH_3,[1] CH_3 and CH_2CH_3,[15] and also Cl and N_2[13]), especially in cases when the crystal packing is dominated by the supporting ligand system. These examples clearly indicate that accurate determinations of correct bond lengths require great care to be taken to ensure that the *crystal* which is examined is pure. This may be a task of considerable difficulty to verify, especially if the nature of the potential impurity is unknown.

Experimental Section

General Considerations. All manipulations were performed with a combination of glovebox, high-vacuum, or Schlenk techniques.[16] Solvents were purified and degassed by standard procedures. NMR spectra

(14) Furthermore, reactions of Grignard reagents frequently result in halide exchange in addition to alkyl exchange. For example, see: (a) Hessen, B.; Lemmen, T. H.; Luttikhedde, H. J. G.; Teuben, J. H.; Petersen, J. L.; Huffman, J. C.; Jagner, S.; Caulton, K. G. *Organometallics* **1987**, *6*, 2354–2362. (b) Han, R.; Bachrach, M.; Parkin G. *Polyhedron* **1990**, *9*, 1775–1778.

(15) Schrock, R. R.; Kolodziej, R. M.; Liu, A. H.; Davis, W. M.; Vale, M. G. *J. Am. Chem. Soc.* **1990**, *112*, 4338–4345.

(16) (a) McNally, J. P.; Leong, V. S.; Cooper, N. J. *A.C.S. Symp. Ser.* **1987**, *357*, 6–23. (b) Burger, B. J.; Bercaw, J. E. *A.C.S. Symp. Ser.* **1987**, *357*, 79–97.

Table IV. Unit Cell Parameters for $\{\eta^3\text{-HB(3-Bu}^t\text{pz)}_3\}\text{ZnX}_{1-n}\text{Y}_n$

n	0	0.02	0.11	0.29	0.50	0.62	0.82	1.0
				$\{\eta^3\text{-HB(3-Bu}^t\text{pz)}_3\}\text{ZnCl}_{1-n}\text{I}_n$				
a (Å)	16.029 (5)	16.052 (3)	16.087 (3)	16.166 (3)	16.255 (3)	16.294 (4)	16.400 (5)	16.443 (3)
b (Å)	15.975 (5)	15.995 (4)	15.970 (4)	15.929 (4)	15.899 (4)	15.870 (5)	15.880 (6)	15.848 (5)
c (Å)	9.786 (2)	9.794 (2)	9.791 (1)	9.817 (1)	9.857 (1)	9.863 (2)	9.916 (2)	9.927 (2)
U (Å^3)	2506 (1)	2515 (1)	2515 (1)	2528 (1)	2547 (1)	2551 (1)	2583 (1)	2587 (1)

n	0	0.07	0.07	0.08	0.69	0.91	1.0
			$\{\eta^3\text{-HB(3-Bu}^t\text{pz)}_3\}\text{Zn(CH}_3)_{1-n}\text{I}_n$				
a (Å)	16.297 (4)	16.336 (3)	16.326 (3)	16.329 (3)	16.395 (3)	16.416 (3)	16.443 (3)
b (Å)	15.882 (4)	15.902 (4)	15.903 (3)	15.891 (3)	15.858 (4)	15.835 (4)	15.848 (5)
c (Å)	9.757 (2)	9.781 (1)	9.787 (1)	9.776 (1)	9.880 (2)	9.915 (2)	9.927 (2)
U (Å^3)	2525 (1)	2541 (1)	2541 (1)	2537 (1)	2569 (1)	2577 (1)	2587 (1)

n	0	0.12	0.36	0.44	0.46	0.54	1.0
			$\{\eta^3\text{-HB(3-Bu}^t\text{pz)}_3\}\text{Zn(CH}_3)_{1-n}\text{Cl}_n$				
a (Å)	16.297 (4)	16.275 (4)	16.192 (2)	16.192 (2)	16.192 (2)	16.158 (3)	16.029 (5)
b (Å)	15.882 (4)	15.904 (5)	15.908 (4)	15.932 (3)	15.939 (4)	15.937 (4)	15.975 (5)
c (Å)	9.757 (2)	9.760 (2)	9.757 (1)	9.777 (1)	9.772 (2)	9.777 (2)	9.786 (2)
U (Å^3)	2525 (1)	2526 (1)	2513 (1)	2522 (1)	2522 (1)	2518 (1)	2506 (1)

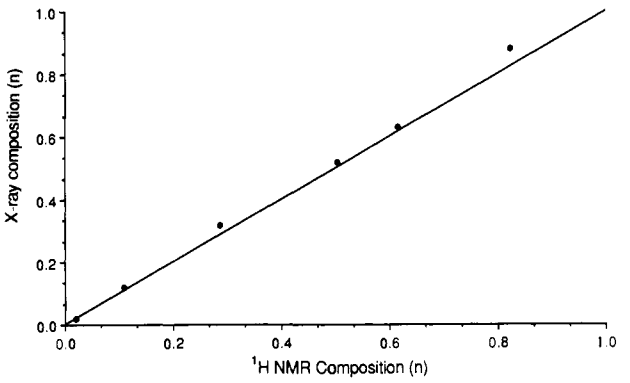

Figure 7. Comparison of the composition of $\{\eta^3\text{-HB(3-Bu}^t\text{pz)}_3\}\text{ZnCl}_{1-n}\text{I}_n$ as determined by ^{1}H NMR analysis and by refining occupancies. For reference, the line drawn with a slope of unity represents perfect agreement.

were measured on a Varian VXR 400 spectrometer. $\{\eta^3\text{-HB(3-Bu}^t\text{pz)}_3\}\text{ZnX}$ (X = Cl, Br, I, CH_3) were prepared as described elsewhere.[9] Crystals of the pure complexes and mixtures were obtained from concentrated solutions of dichloromethane or THF at room temperature. After X-ray data collection, the composition of each crystal was determined by ^{1}H NMR spectroscopy. In most cases similar compositions were also measured for the bulk sample, although in some cases deviations were observed.

X-ray Structure Determination Procedures. Crystal data, data collection, and refinement parameters for the pure complexes $\{\eta^3\text{-HB(3-Bu}^t\text{pz)}_3\}\text{ZnX}$ (X = Cl, Br, I, CH_3) are summarized in Table III. Complete tables of crystal data, data collection, and refinement parameters are given in the supplementary material. Unit cell parameters for all structures are given in Table IV. A typical procedure for the structure determination is as follows. A single crystal was mounted in a glass capillary and placed on a Nicolet R3m diffractometer. The unit cell was determined by the automatic indexing of 25 centered reflections and confirmed by examination of the axial photographs. Intensity data were collected with graphite monochromated Mo Kα X-radiation (λ = 0.71073 Å). Check reflections were measured every 100 reflections, and the data were scaled accordingly and corrected for Lorentz, polarization, and absorption effects. The structure was solved with direct methods and standard difference map techniques on a Data General NOVA 4 computer with SHELXTL.[17] Systematic absences were consistent with the space groups *Pnma* or $Pna2_1$, but consideration of the E value statistics suggested the choice *Pnma* (no. 62). Most of the hydrogen atoms were located in the difference map after all the non-hydrogen atoms were located and refined anisotropically, but hydrogens on carbon were allowed to refine in calculated positions (d_{C-H} = 0.96 Å; $U_{iso}(H) = 1.2U_{iso}(C)$). The composite "atom" at the disordered site was modeled by refining each atom of the composite pair with the constraint that their positional and anisotropic thermal parameters maintained common values, while the site occupancies were allowed to refine subject to the constraint that their sum was 0.5 (the disordered site lies on a mirror plane). The success of this treatment is illustrated by Figure 7, which shows the results for the series $\{\eta^3\text{-HB(3-Bu}^t\text{pz)}_3\}\text{ZnCl}_{1-n}\text{I}_n$, indicating how excellent agreement is observed between the composition as determined by refining the site occupancies and the composition as determined by NMR spectroscopy. Selected bond lengths and angles for the pure complexes $\{\eta^3\text{-HB(3-Bu}^t\text{pz)}_3\}\text{ZnX}$ (X = Cl, Br, I, CH_3) are given in Table I, while complete tables of atomic coordinates, bond distances and angles, anisotropic displacement parameters, and ORTEP drawings for all structures are given in the supplementary material.

Acknowledgment. This work was supported by the National Science Foundation (CHE-9007512). We thank two of the reviewers for valuable comments. G.P. is the recipient of an A. P. Sloan Research Fellowship (1991–1993) and a Camille and Henry Dreyfus Teacher-Scholar Award (1991–1996).

Supplementary Material Available: Tables of crystal and intensity collection data, atomic coordinates, bond distances and angles, anisotropic displacement parameters, and ORTEP drawings for all structures (141 pages). Ordering information is given on any current masthead page.

(17) Sheldrick, G. M. SHELXTL, An Integrated System for Solving, Refining, and Displaying Crystal Structures from Diffraction Data; University of Gottingen, Göttingen, Federal Republic of Germany, 1981.